COVER SHEET

NOTE: This coversheet is intended for you to list your article title and author(s) name only

—this page will not appear on the CD-ROM.

Paper Number: 265

Title: **Simulating matrix crack and delamination interaction in a clamped tapered beam**

Authors: N.V. De Carvalho
B.R. Seshadri
J.G. Ratcliffe
G.E. Mabson
L.R. Deobald

ABSTRACT

Blind predictions were conducted to validate a discrete crack methodology based on the Floating Node Method to simulate matrix-crack/delamination interaction. The main novel aspects of the approach are: (1) the implementation of the floating node method via an "extended interface element" to represent delaminations, matrix-cracks and their interaction, (2) application of directional cohesive elements to infer overall delamination direction, and (3) use of delamination direction and stress state at the delamination front to determine migration onset.

Overall, good agreement was obtained between simulations and experiments. However, the validation exercise revealed the strong dependence of the simulation of matrix-crack/delamination interaction on the strength data (in this case transverse interlaminar strength, Y_T) used within the cohesive zone approach applied in this work. This strength value, Y_T, is itself dependent on the test geometry from which the strength measurement is taken. Thus, choosing an appropriate strength value becomes an ad-hoc step. As a consequence, further work is needed to adequately characterize and assess the accuracy and adequacy of cohesive zone approaches to model small crack growth and crack onset. Additionally, often when simulating damage progression with cohesive zone elements, the strength is lowered while keeping the fracture toughness constant to enable the use of coarser meshes. Results from the present study suggest that this approach is not recommended for any problem involving crack initiation, small crack growth or multiple crack interaction.

N.V. De Carvalho and B.R. Seshadri, National Institute of Aerospace, 100 Exploration Way, Hampton, VA, 23666.
J.G. Ratcliffe, Durability, Damage Tolerance and Reliability Branch, MS 188E, NASA Langley Research Center, Hampton, VA, 23681, U.S.
G.E. Mabson, Boeing Research and Technology, Seattle, WA, 98124
L.R. Deobald, Boeing Commercial Airplanes, Seattle, WA, 98124

INTRODUCTION

As part of the NASA Advanced Composites Project (ACP), the clamped tapered beam specimen, illustrated in Figure 1, has been designed to provide validation data for progressive damage analysis models [1]. The present work reports on blind predictions performed with a 3D discrete crack approach based on the Floating Node Method (FNM) [2], of the quasi-static simulation of the clamped tapered beam.

The Clamped Tapered Beam (CTB) specimen is based on the delamination migration test proposed in [3, 4]. The tapered geometry was devised to localize the first damage occurrence in the tapered region, without prescribing an initial crack. The specimen is clamped on both ends and loaded via a pin, connected to a loading rod, located at a distance L_A or L_B from the left-hand-side clamp, as shown in Figure 1. The boundary and loading conditions were chosen to favor delamination growth and subsequent migration after a certain amount of delamination growth. The typical sequence of events consists of the onset of a matrix-crack at the tapered region which triggers delamination, followed by subsequent delamination migration to a different interface via a dominant matrix-crack. Varying the load-offset application point from L_A to L_B affects both the peak load and the migration location. The specimen was designed to ensure that the fatigue crack growth would reside in the Paris Law crack growth regime of IM7/8552 Carbon Fiber Reinforced Plastic (CFRP) for the duration of a complete set of damage events (matrix-crack initiation, delamination, migration, etc.), thus avoiding premature damage arrestment or unstable failure. Further details of the specimen and design considerations are given in [1].

In the present work an approach based on the FNM is assessed. The FNM represents discrete crack networks by generating sub-elements within cracked finite elements through the use of floating nodes [2]. No *a priori* location for damage initiation is assumed. As proposed, the methodology does not limit the number of possible matrix-cracks, delaminations, or the crack spacing, thereby enabling the model to accommodate the initiation and propagation of complex crack networks at the meso-scale without the need for re-meshing. For models under quasi-static loading, the FNM approach is combined with Directional Cohesive Zone Elements (DCZE) to model onset and growth of delamination and matrix-cracks.

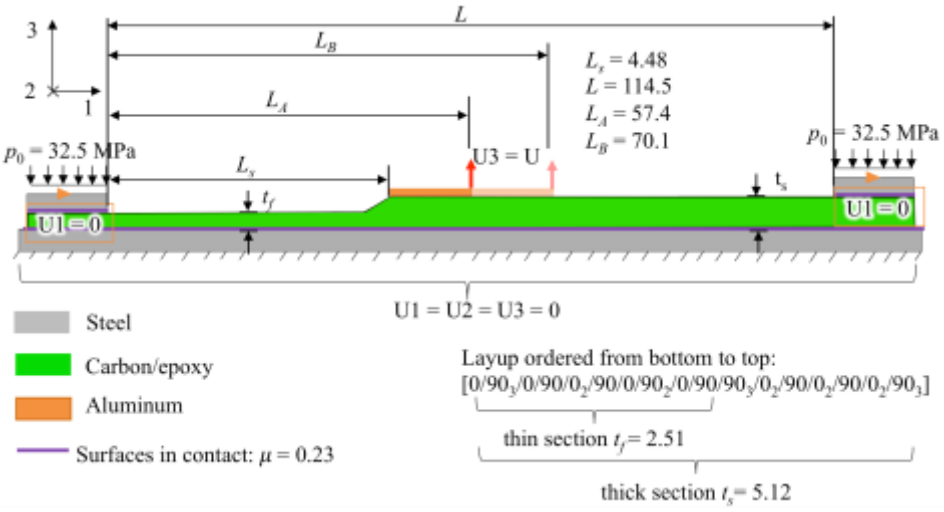

Figure 1. Clamped tapered beam specimen and boundary conditions.

METHODOLGY

In this section the methodology used in the blind-predictions exercise will be outlined, with emphasis on the extended interface floating node element developed, the directional cohesive zone elements, and the migration onset criterion.

Floating Node Method extended interface element

An extended interface element has been used to capture the damage morphology in the central region of the CTB specimen. It consists of a 3D 48-node element, composed of 16 nodes (named real) which have pre-assigned positions, and 32 floating nodes (Figure 2a). The real nodes are used to define two sub-elements: one above and another below a pre-assigned cohesive element located at the interface between the two sub-elements - hence the name "extended interface" element. The 32 floating nodes are the minimum subset of floating nodes that enable the two sub-elements to split independently. The floating nodes have their topological relationships to the element assigned in the same manner as regular nodes, and are included in the element connectivity list. However, if the element is not split, their degrees of freedom are not activated, and they can be removed from the system of equations. If the sub-elements need to be split to accommodate matrix-cracks, the floating nodes are used as required. Since the connectivity of the floating nodes is defined 'a priori', when activated, they automatically enforce crack path continuity. For example, an edge will be split by a unique pair of floating nodes shared by all the elements sharing that edge, as defined by their connectivity list. The element, as proposed, can be used to represent matrix-cracks with any orientation in the *xy* plane (Figure 2). As matrix-cracks initiate, Figure 2b, the interface element may also split using floating nodes, and cohesion elements are assigned as required to model the subsequent opening of the newly generated splits. The correct representation of the kinematics has been demonstrated to be an important feature to correctly capture matrix-crack/delamination interaction [2, 5].

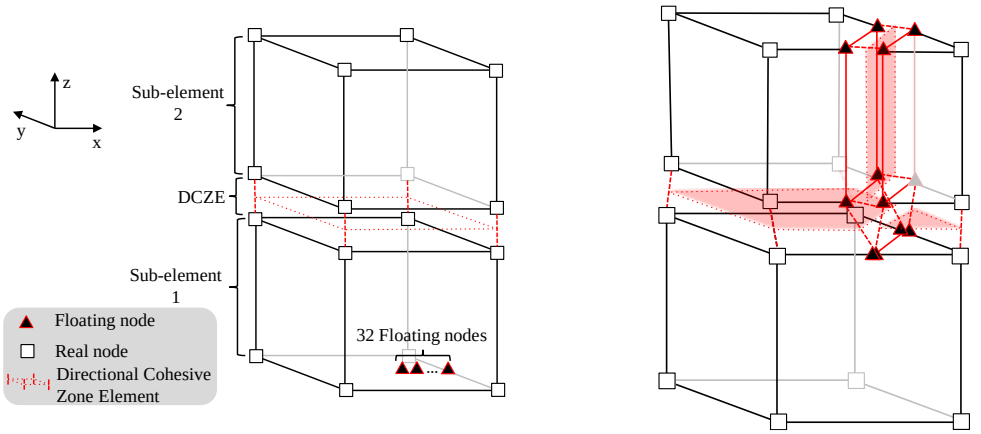

(a) Pristine extended interface element with sub-elements above and below a Directional Cohesive Zone Element (DCZE).

(b) element representing a single matrix-crack

Figure 2. Extended interface element. Distances between between sub-elements and partitions are exaggerated for illustration purposes.

Matrix-cracks and through-thickness straight crack approximations

As depicted in Figure 2b, the matrix-cracks are assumed to be straight through the ply thickness. This approximation is used to facilitate the integration of partitioned elements. However, matrix-cracks will only be straight through-thickness, as depicted in Figure 2b, if forming under transverse tensile loads; otherwise their angle may vary, see Figure 3. In order to attenuate the effect of this approximation, the present study uses two corrections. The first consists in determining the cohesive tractions in a rotated coordinate system, following [6, 7]. In addition, since the matrix-cracks are free to seek a mode I path as they propagate through-thickness, the shear component determined along direction 1 in Figure 3 is ignored, if not zero, and not considered to contribute to the mode-mixity.

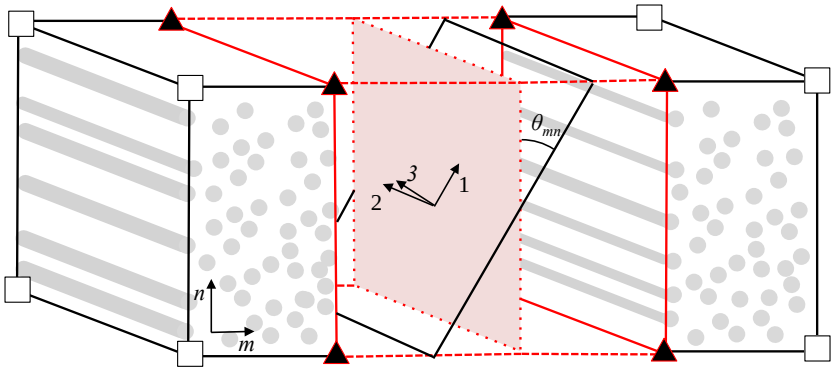

Figure 3. Matrix-crack through thickness approximation.

Matrix-cracks are considered to onset via the Benzeggagh-Kenane (BK) criterion, written in traction space [8], when the effective traction:

$$(\tau_e)^2 = (\langle\sigma_3\rangle)^2 + (\tau_{sh})^2\beta^\eta \tag{1}$$

exceeds the strength, given by:

$$(Y_M)^2 = (Y_T)^2 + (Y_S)^2\beta^\eta \tag{2}$$

where $\tau_{sh} = \sqrt{(\tau_1)^2 + (\tau_2)^2}$ and $\langle x\rangle$ is defined as $\langle x\rangle = \frac{1}{2}(x + |x|)$, and Y_T and Y_S designate the transverse and shear strength, respectively; η is a fitting parameter; and β is the mode-mixity which is assumed, for matrix-cracks, to be given, by:

$$\beta = \frac{\langle\sigma_3\rangle}{\sqrt{(\tau_2)^2 + (\langle\sigma_3\rangle)^2}} \tag{3}$$

The tractions are determined in the plane perpendicular to the maximum principal stress obtained in the '*mn*' plane transverse to the fibers (hence $\tau_1 = 0$), Figure 3. In addition, matrix-cracks can also be onset via the migration criterion that will be outlined later in this section. As mentioned previously, once a matrix-crack onsets and a given element is split, a cohesive element is automatically inserted and, if sufficient

traction is applied, it will subsequently open according to its traction-separation law. The mixed-mode traction separation law implemented is based on the formulation proposed in [8]. Using Eqs. 1 and 2 to determine matrix-crack onset ensures consistency throughout the crack onset, insertion and subsequent opening process, since Eqs. 1 and 2 are also used in [8] to determine the peak of the bi-linear traction-separation law.

Directional cohesive elements - active ply determination

Directional cohesive elements are used to estimate the delamination growth direction. This information is in turn used to determine the ply towards which delamination tends to grow, here named as the "activated ply" [9]. We assume the crack growth direction vector **d** is opposite to the gradient of the displacement jump δ_T determined within the element:

$$\mathbf{d} = -\nabla\delta_T \tag{4}$$

where:

$$\delta_T = \sqrt{\delta_1^2 + \delta_2^2 + \langle\delta_3\rangle^2} \tag{5}$$

and δ_i are the shear and normal displacement jump components. The gradient $\nabla\delta_T$ is computed at the centroid, $\mathbf{x}_c$, of the element using the element shape functions:

$$\mathbf{d}^T = -\frac{\partial\delta_T(\mathbf{x}_c)}{\partial\mathbf{x}} \tag{6}$$

In the present work, delamination growth direction is used in conjunction with shear traction vector $\boldsymbol{\tau}$:

$$\boldsymbol{\tau} = \frac{\{\tau_1, \tau_2\}}{\sqrt{\tau_1^2 + \tau_2^2}} \tag{7}$$

to determine the activated ply. This procedure is illustrated in Figure 4 and it assumes that microcracks form ahead of the delamination, with an orientation governed by the principle tensile stress. Therefore, knowing the crack direction, **d**, and the shear traction direction, $\boldsymbol{\tau}$, the activated ply can be determined by:

$$\begin{cases} \boldsymbol{\tau}\cdot\mathbf{d} > 0.0 & : \text{lower ply is activated} \\ \boldsymbol{\tau}\cdot\mathbf{d} < 0.0 & : \text{upper ply is activated} \end{cases} \tag{8}$$

as graphically illustrated in Figure 4. If $\boldsymbol{\tau}\cdot\mathbf{d}$ is positive, the ply below the interface element is activated, otherwise the ply above is considered to be activated. If $\boldsymbol{\tau}\cdot\mathbf{d} = 0$, both plies are considered to be activated. The criterion above assumes a stress normal to the interface, $\sigma \geq 0$. If $\sigma < 0$, the orientation of the matrix-cracks will

rotate, and the criterion will be inversed, i.e., if $\boldsymbol{\tau}.\mathbf{d}$ is positive, the ply above the interface is activated, and if $\boldsymbol{\tau}.\mathbf{d}$ is negative the ply below is activated.

In the present work, the information regarding an activated ply is used to determine propensity for migration. It is envisaged that in future studies this information can also be used to adjust for different mixed-mode fracture toughness values as a function of activated ply, e.g., in tape/fabric interfaces [10].

The cohesive zone elements' constitutive response follows [8]. One aspect worth noting of such formulation is the requirement that:

$$Y_S = Y_T \sqrt{\frac{G_{IIc}}{G_{Ic}}} \tag{9}$$

where G_{Ic} and G_{IIc} are the Mode I and II fracture toughness, respectively, which ensures that large crack growth under mode-mixed conditions is accurately predicted. However, as a consequence, Eq. 9 may limit the ability of the approach to accurately capture damage initiation and small crack growth, since the actual material properties may not relate as given in Eq. 9.

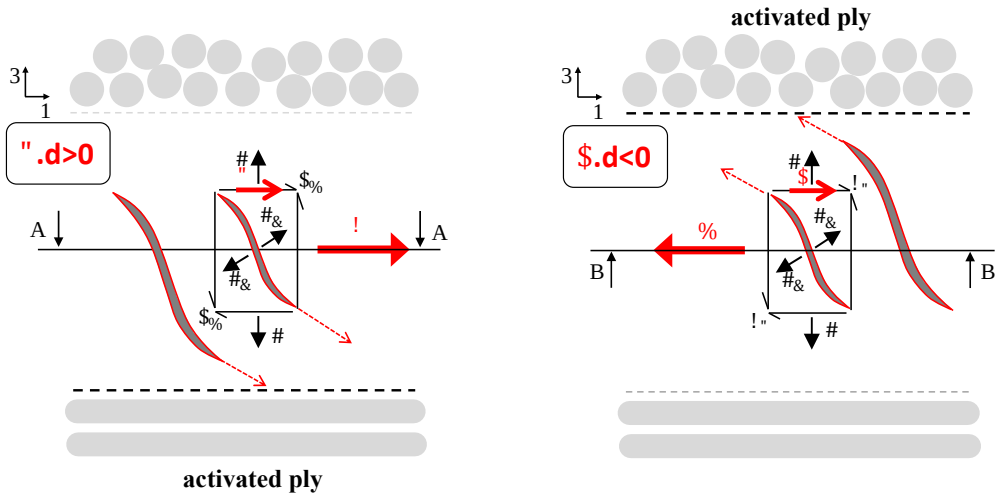

(a) bottom ply activated

(b) top ply activated

Figure 4. Determination of activated ply as a function of crack and shear traction vector direction.

Migration onset

Migration onset in the CTB specimen is defined as the onset of a dominant matrix-crack that kinks out of the plane of its originating delamination, towards a different ply interface. In the current analysis, migration onset is modeled by splitting elements and inserting cohesive elements along the predicted crack surface (or path). The criterion for migration onset consists of comparing microcrack growth direction to the fiber direction of an active ply, $\mathbf{f}_a$. Since it is known that the in-plane orientation of the microcracks is perpendicular to the shear traction vector (in-plane), the microcracks are assumed to have a propensity for meandering through the active ply if:

$$|\boldsymbol{\tau} \cdot \mathbf{f}_a| < \cos \gamma_{cr} \tag{10}$$

where γ_{cr} is used to define a range of relative orientations between $\boldsymbol{\tau}$ and $\mathbf{f}_a$ that may lead to migration. This criterion is illustrated in Figure 5, for the case depicted in Figure 4. Figure 5a illustrates a case in which the criterion proposed in Eq. 10 is not met. Indeed, for migration onset to occur in this case, the microcracks would need to either break fibers or rotate by 90° as they grow into the activated ply. Figure 5b represents a case where Eq. 10 is met. In this case, the relative orientation of the matrix-cracks to the activated ply fiber direction is such that the microcracks are assumed to be able to meander through the activated ply. Although the value for $\gamma_{cr} = 30^{\circ}$ used in this study is based on the conditions for containment observed in [11], γ_{cr} is considered to be a numerical parameter that serves to prevent spurious insertion of matrix-cracks, while guaranteeing the delamination and migration onset are treated as part of the same process, as observed experimentally. The condition above is assessed as the traction at the cohesive element located at the interface equals the strength. If the criterion is met, cohesive elements are inserted through-thickness, splitting the sub-element. The opening of these cohesive elements, as well as the subsequent opening of the also-split interface cohesive element is governed by their traction-separation law. Hence, migration will only be completed if it is energetically favorable. During that assessment, the in-plane failure criterion is deactivated in the element being assessed. Once migration onsets, it is assumed to grow through the thickness with an angle of $\theta_{nm} = 45°$ relative to the delamination growth direction.

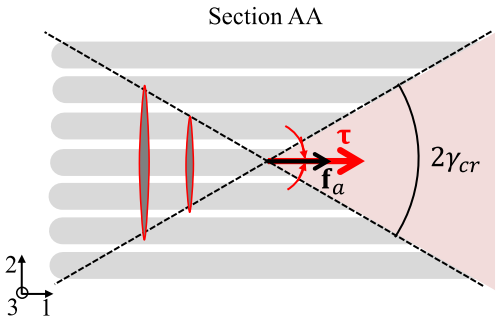

(a) In-plane view of activated ply of Figure 4a.

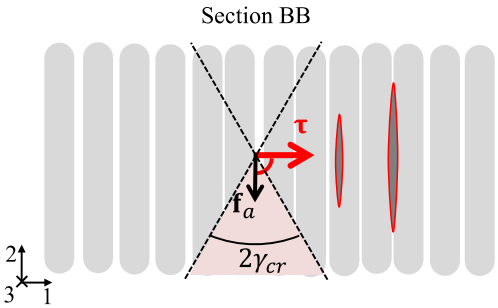

(b) In-plane view of activated ply of Figure 4b.

Figure. 5 Illustration of migration onset criterion, Eq. 10. The criterion is met in (b) and not met in (a). In (a) the microcracks would need to either break fibers or rotate by 90° to grow into the activated ply, while in (b) the microcracks are able to meander through the activated ply with less changes to their path.

NUMERICAL MODEL AND MATERIAL PROPERTIES

The boundary conditions for the model were chosen based on the best fit to Digital Image Correlation (DIC) data. Further details on this procedure are given in [1]. The boundary conditions consist of pressure applied at the clamp region in a first step, followed by displacement applied at a line of nodes along the hinge as illustrated in Figure 1. The material properties used are summarized in Tables I and II. Two values of Y_T are reported in the table. These two values define lower and upper bounds of material strength values as measured by 90° tensile or 3-point bend tests, and will be used to assess the sensitivity of the solution on Y_T.

TABLE I. ELASTIC PROPERTIES [12].

E_{11} [GPa]	E_{22} [GPa]	E_{33} [GPa]	G_{12} [GPa]	G_{13} [GPa]	G_{23} [GPa]	ν_{12}	ν_{13}	ν_{23}
157.2	8.96	8.96	5.08	5.08	2.99	0.32	0.32	0.5

TABLE II. STRENGTH AND FRACTURE TOUGHNESS PROPERTIES

Y_T [MPa]	Y_S [MPa]	G_{Ic} [N.mm^{-1}]	G_{IIc} [N.mm^{-1}]	η
{64 [13], 127 [14]}	{112, 223}	0.24 [15]	0.739 [16]	2.1 [17]

Following [8], the values for Y_S are assumed to be given by Eq. 9. As mentioned previously, while Eq. 9 guarantees the cohesive zone approach implemented is capable of modeling large crack propagation under mixed-mode conditions, it may limit its accuracy in the modeling of crack initiation and small crack growth, particularly for shear dominated cracks, since the actual material properties may not relate as given in Eq. 9. Intra-laminar and inter-laminar strength and toughness properties are assumed to be the same.

The finite element mesh used for the blind-predictions is illustrated in Figure 6. The floating node extended interface element was used to model damage onset and propagation in the center region of the laminate, (Figure 6). The remainder of the specimen was modeled with a combination of solid (C3D8I) and shell (SC8R) Abaqus® elements. A mesh refinement study was performed for both Y_T = 64 MPa and Y_T = 127 MPa, focusing on mesh convergence of the peak load value. This study showed that the peak load predictions obtained by halving the element size, $el_x \approx 0.04$ mm and $el_y \approx 0.045$, differed from the predictions obtained with the mesh illustrated in Figure 6 by less than 3%, and hence the solution was considered to have converged.

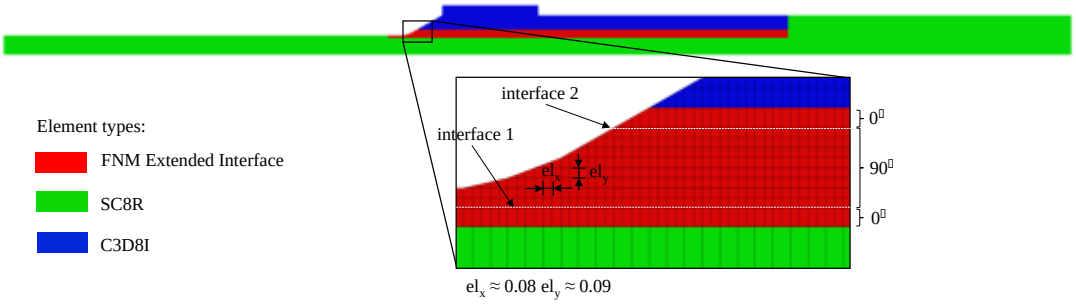

Figure 6. Mesh size and element selection

BLIND PREDICTION RESULTS

The sequence of events observed experimentally consists of an initial matrix-crack that develops between interfaces 1 and 2 within the taper region. That crack transitions into a delamination that grows along “interface 1” and migrates up via a matrix-crack to “interface 2”. This sequence of events was correctly simulated as illustrated in Figure 7. The main difference between simulated and observed damage events was the initial matrix-crack location, which was predicted near interface 2, at the weak singularity, in the taper region. The simulations also predicted multiple

migration attempts prior to the final migration. Although these could not be observed at the edge of the specimens tested, X-ray images of tested specimens revealed migration attempts at the center of the specimens [1].

The blind-predictions for static loading are shown in Figure 8, together with the experimental load-displacement data. Two simulations, corresponding to assumed transverse tensile material strengths of Y_T = 64 and 127 MPa, are depicted by red and black lines, respectively. These two values define lower and upper bounds of material strength values as measured by 90° tensile or 3-point bend tests, respectively [13, 14]. As can be observed, the simulations showed a strong dependence on the assumed Y_T. In both cases, damage initiation is predicted in the 90° ply near interface 2, at the weak singularity.

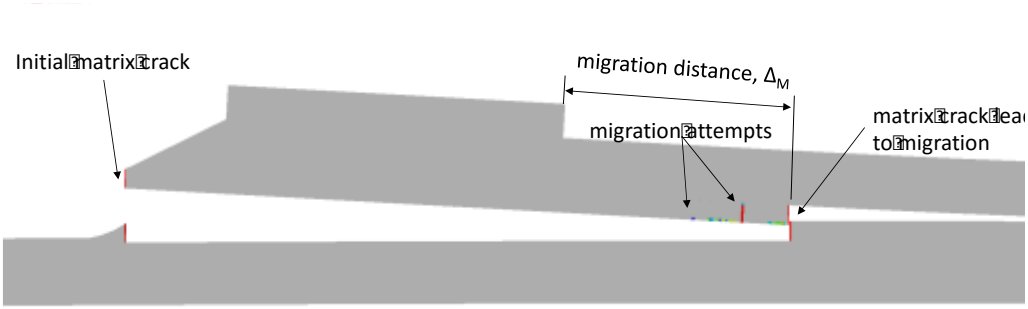

Figure 7. Final simulated damage state, obtained with Y_T =127 MPa. Red represents elements completely opened.

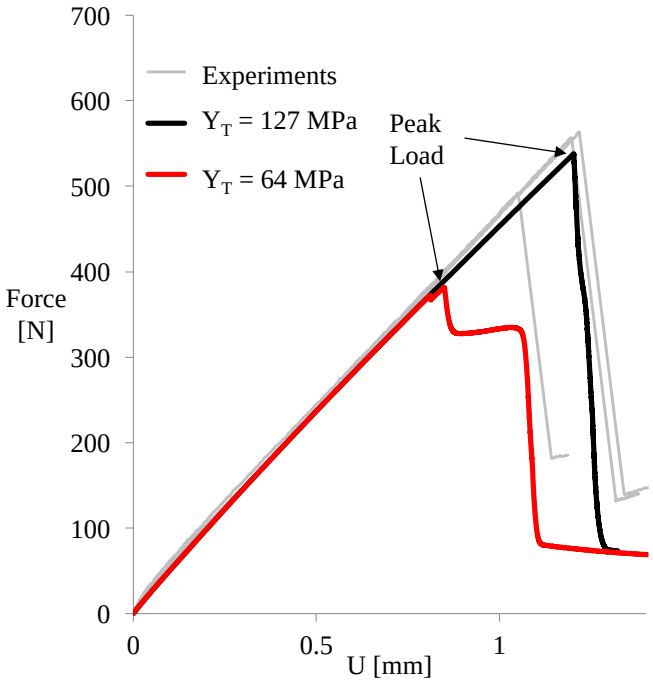

Figure 8. Comparison of the load-displacement experimental response to simulations obtained with Y_T = 64 and Y_T = 127 MPa.

The blind-predictions for migration location are compared with experimental data in Figure 9. Results from blind predictions are shown for the two transverse strength

values of Y_T = 64 and 127 MPa. Migration location is measured from the load application point, as depicted in Figure 7. Simulations show that migration location occurs at greater distance from the load application point for Y_T = 64 compared to the results obtained assuming Y_T = 127 MPa.

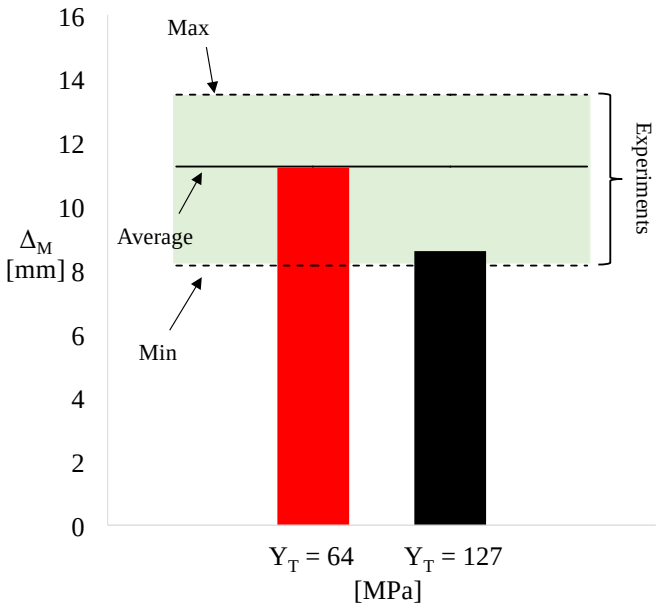

Figure 9. Comparison of migration location obtained from the experiments and the simulated migration location obtained with Y_T = 64 and Y_T = 127 MPa.

Overall, the results correlate well with the experiments. The peak load prediction obtained with higher Y_T was closer to that experimentally obtained. The prediction obtained with Y_T = 64 resulted in a significantly lower peak load prediction. However, in the taper region, the "as manufactured geometry" was different from the geometry idealized in the current analysis, as highlighted in Figure 10. Hence, the better agreement alone may not necessarily indicate Y_T = 127 MPa is a more adequate transverse strength value. The migration process was also seen to be affected by the transverse tensile strength. In this case the migration distance corresponding to Y_T = 64 MPa was closer to the average migration distance measured experimentally. However, the migration distance obtained with Y_T = 127 MPa was also within the experimental scatter.

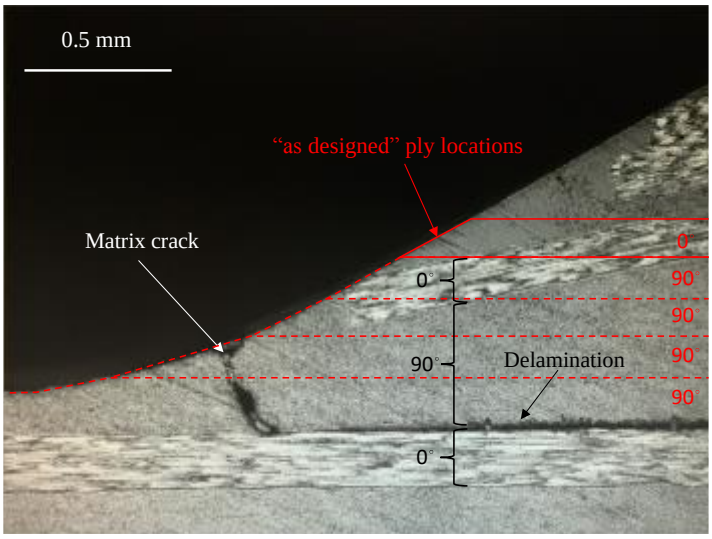

Figure 10. Qualitative comparison between the "as manufactured" and the "as designed" ply location near the taper region.

SENSITIVITY STUDY: EFFECT OF Y_T

In this section, the effect of strength on the peak load and migration location are further investigated and discussed. To do so, an additional simulation with Y_T = 32 MPa was performed, and the results obtained compared with the results obtained previously for Y_T = {64, 127} MPa.

Figure 11 compares the peak load predictions obtained assuming Y_T = {32, 64, 127} MPa. As can be seen, the peak load is very mildly affected by Y_T below 64 MPa. This indicates that for Y_T lower than 64 MPa the onset is controlled by the fracture toughness.

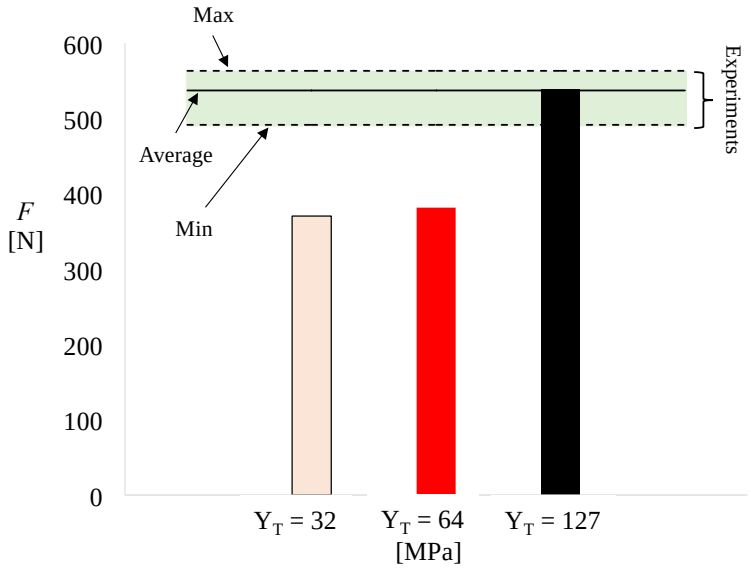

Figure 11. Variation in peak load prediction with Y_T.

The effect of Y_T on migration location is particularly interesting, since crack deflection or kinking is often treated in brittle materials using Linear Elastic Fracture

Mechanics (LEFM) based kinking criteria [18, 19]. In Figure 12, the migration location results obtained with Y_T = {32, 64, 127} MPa are compared. The results show that despite the apparent similarity in peak load, Y_T = 32 and Y_T = 64 MPa lead to significant differences in migration location prediction. Additionally, while a lower Y_T = 32 MPa leads to a conservative prediction in terms of peak load, it provides a non-conservative prediction in terms of migration location. The simulated damage state obtained with Y_T = 32 MPa and Y_T = 127 MPa, Figures 7 and 13, respectively, are also markedly different. With Y_T = 32 MPa, prior to migration, a region of partially opened elements, is obtained, whereas with Y_T = 127 MPa, only a few isolated migration attempts are observed. This finding indicates that the delay in crack migration is associated with the development of a migration attempt region with partially opened elements, akin to a process zone, prior to migration. The development of this process zone, composed of multiple partially opened elements, is originated by the reduction of strength while the fracture toughness remains constant. This is revealed in the present approach by not limiting the number of matrix-cracks and/or their spacing. In doing so, the methodology enables a more realistic material response and provides additional insight regarding the adequacy of the material properties/parameters used.

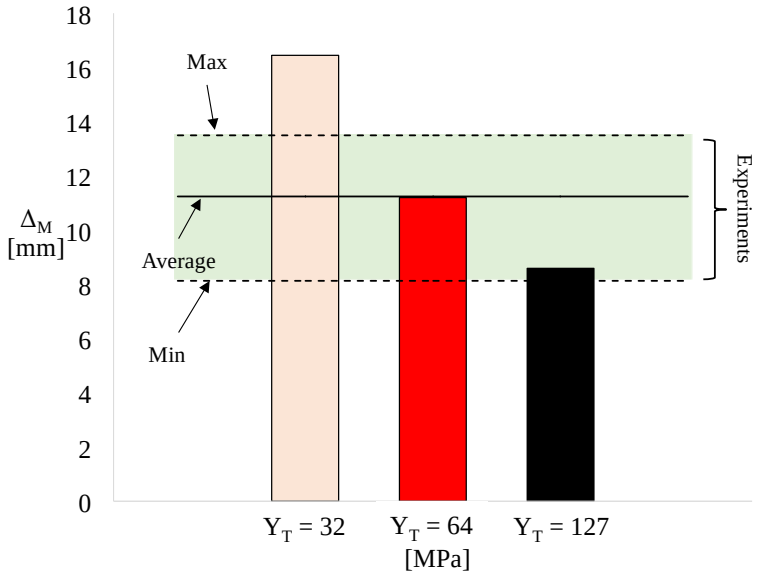

Figure 12. Variation in migration location with Y_T.

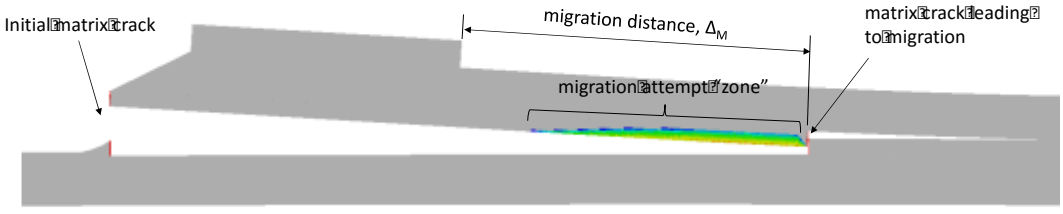

Figure 13. Final simulated damage state, obtained with Y_T = 32 MPa. Red represents elements completely opened.

SUMMARY

As part of the NASA Advanced Composites Project (ACP), the clamped tapered beam specimen has been designed to provide validation data for progressive damage analysis models. The present work focused on the results obtained with a 3D discrete crack approach based on the Floating Node Method. The approach used provided adequate agreement with experimental measurements and shows potential in accurately simulating matrix-crack/delamination interaction. Three key components are identified in order to be able to model matrix-crack/delamination interaction:

- accurately represent the kinematics of the matrix-crack/delamination interaction
- model the matrix-crack angle and its through-thickness mode I propagation
- recognize delamination and matrix-crack interaction are part of the same damage process and model them as such, rather than as separate independent events/damage modes.

While fair qualitative agreement may be obtained with different degrees of approximation to any of the three components highlighted above, e.g. [4, 19, 20, 21, 22], an accurate predictive strategy should aim at considering all of them. In the methodology used, of the three components identified above, the approximation used when modeling angled matrix-cracks and subsequent propagation through-thickness is recognized as the main aspect requiring further evaluation.

The blind predictions also revealed challenges associated with obtaining characterization data for high-fidelity meso-scale modeling frameworks using cohesive zone crack approaches. Particular attention was given to Y_T as a result of its effect on peak-load predictions. Results suggest that the choice of Y_T may not only affect the peak load predictions but also, and even more significantly, affect matrix-crack delamination interaction, which in turn may lead to an incorrect simulation of progressive damage.

A wide range of values for Y_T can be found in literature, as well as evidence of its volume dependency [16], which may undermine the experimental determination of a single value for Y_T. In the present work, values of Y_T leading to good qualitative and quantitative response were found to be high (~ 127 MPa) and pose challenges regarding the size of elements needed when using cohesive zone approaches, and hence its practical application.

While lower values of Y_T may provide conservative estimates of initial crack onset, they may also lead to incorrect simulation of crack interaction and hence erroneous post-peak predictions. This observation suggests that the commonly used approach of lowering the strength while keeping the fracture toughness constant, to enable the use of coarser meshes when simulating damage (in particular delamination) with cohesive zone elements, is not recommended in the predictive simulation of any component where crack initiation, small crack growth, and multiple crack interaction may occur.

REFERENCES

1. Ratcliffe, J.G., Deobald, L., Mabson, G. and N.V. De Carvalho. 2017. "A Clamped Tapered Beam Test to Study Matrix Crack Initiation and Delamination Migration in a Cross-ply Tape Laminate," NASA-TM-2017-219623.
2. Chen, B.Y., Pinho, S.T, De Carvalho, N.V., Baiz, P.M. and T.E. Tay. 2014. "A Floating Node Method for the Modelling of Discontinuities in Composites," *Engineering Fracture Mechanics*, 27:104-134.
3. Ratcliffe, J.G., Czabaj, M.W. and T.K. O'Brien. 2013. "A Test for Characterizing Delamination Migration in Carbon/Epoxy Tape Laminates," NASA/TM–2013-218028.
4. Ratcliffe, J.G. and N.V. De Carvalho 2014. "Investigating Delamination Migration in Composite Tape Laminates," NASA/TM–2014-218289.
5. Chen, B.Y., Tay, T.E., Pinho, S.T. and V.B.C. Tan. 2017. "Modelling delamination migration in angle-ply laminates," *Composites Science and Technology*, 142:145-155.
6. Kawashita, L.F., Pernice, M.F. and S.R. Hallett. 2013. "Mesh-Independent Cohesive Crack Model for the Analysis of Transverse Matrix Cracks in Laminated Composites," presented at IV ECCOMAS Thematic Conference on the Mechanical Response of Composites, 25 - 27 September, 2013.
7. Steenstra, W., van der Meer, F.P. and L.J. Sluys. 2015. "An efficient approach to the modeling of compressive transverse cracking in composite laminates," *Composite Structures*, 128:115-121.
8. Turon, A., Camanho, P.P., Costa, J., J. Renart. 2010. "Accurate simulation of delamination growth under mixed-mode loading using cohesive elements: Definition of interlaminar strengths and elastic stiffness," *Composite Structures*, 92(8):1857-1864.
9. Greenhalgh, E.S. 2009. "Failure analysis and fractography of polymer composites," in Woodhead Publishing Series in Composites Science and Engineering, 192-194.
10. Dávila, C.G, Leone, F.A., Song, K., Ratcliffe, J.G. and C.A. Rose. 2017. "Material Characterization for the Analysis of Skin/Stiffener Separation," 32nd ASC Technical Conference. West Lafayette, IN.
11. Czabaj, M.W., Davidson, B.D. and J.G. Ratcliffe. 2016. "A Modified Edge Crack Torsion Test for Measurement of Mode III Fracture Toughness of Laminated Tape Composites," 31st ASC Technical Conference, Williamsburg, VA.
12. Makeev, A., Nikishkov, Y., Seon, G. and E. Lee. 2016. "Analysis Methods Improving Confidence in Material Qualification for Laminated Composites," in *Proceedings of the AHS 72nd Annual Forum*, May 17-19, 2016, USA.
13. NIAR Report: NCP-RP-2009-028 Revision A.
14. O'Brien, T.K., Chawan, A.D., DeMarco, K. and I. Paris. 2001. "Influence of Specimen Preparation and Specimen Size on Composite Transverse Tensile Strength and Scatter," NASA/TM-2001-211030.
15. Murri, G.B. 2013. "Evaluation of Delamination Onset and Growth Characterization Methods under Mode I Fatigue Loading," NASA/TM-2013-21766.
16. O'Brien, T.K., Johnston W.M., and G.J. Toland. 2010. "Mode II Interlaminar Fracture Toughness and Fatigue Characterization of a Graphite Epoxy Composite Material," NASA/TM-2010-216838.
17. Ratcliffe, J.G. and W. Johnston. 2014. "Influence of Mixed Mode I-Mode II Loading on Fatigue Delamination Growth Characteristics of a Graphite Epoxy Tape Laminate," 29th ASC Technical Conference, Arlington, TX.
18. He, M-Y. and J.W. Hutchinson 1989. "Kinking of a crack out of an interface," *Journal of Applied Mechanics*, 56:270-278.

19. De Carvalho, N.V., Chen, B.Y., Pinho, S.T., Ratcliffe, J.G., Baiz, P.M. and T.E. Tay. 2015. "Modeling Delamination Migration in Cross-Ply Tape Laminates," *Composites Part A: Applied Science and Manufacturing*, 71:192-203.
20. Adluru, H.K., Hoos, K.H., and V.I. Endel. 2017. "Discrete Damage Modelling of Delamination Migration in Clamped Tapered Laminated Beam Specimens," 32nd ASC Technical Conference, West Lafayette, IN, 2017.
21. Li, X. and J. Chen. 2017. "A highly efficient prediction of delamination migration in laminated composites using the extended cohesive damage model," *Composite Structures* 160:712-721.
22. Adluru, H.K, Hoos, K.H., and E.V. Iarve. 2017. "Discrete Damage Modelling of Delamination Migration in Clamped Tapered Laminated Beam Specimens," 32nd ASC Technical Conference. West Lafayette, IN.